ELSEVIER

Journal of Crystal Growth 194 (1998) 321–330

JOURNAL OF CRYSTAL GROWTH

Combined heat transfer in floating zone growth of large silicon crystals with radiation on diffuse and specular surfaces

Zhixiong Guo[a], Shigenao Maruyama[a,*], Shinji Togawa[b]

[a] *Institute of Fluid Science, Tohoku University, Katahira 2-1-1, Aoba-ku, Sendai 980-8577, Japan*
[b] *Komatsu Electronic Metals Co., Ltd., 2612 Shinomiya, Hiratsuka, Kanagawa 254, Japan*

Received 30 June 1998; accepted 25 August 1998

Abstract

Numerical analyses are conducted to investigate the combined heat transfer in floating zone growth of large Si crystals with needle-eye technique. The radiation element method, REM2, is employed to determine the radiative heat exchange, in which the view factors associated with the components in the float zone furnace and both the diffuse and specular reflection components are incorporated. The boundary element method and the finite difference method are adopted to calculate the electromagnetic field and the heat conduction, respectively. The effect of surface radiative characteristics of Si melt and crystal, i.e., diffuse and/or specular, is discussed in detail. It is found that the consideration of specular surfaces increases the Joulean heat and the radiative heat flux. The temperature fields are obtained for the cases of diffuse and specular, and the difference between the two different cases is obvious in the crystal and molten zone areas. The molten zone is enlarged when the specular surface is accounted for. The interface shape is examined and found to be in good agreement with the experiment. © 1998 Elsevier Science B.V. All rights reserved.

Keywords: Heat transfer; Radiation; Specular reflection; Floating zone growth; Silicon crystal; Joulean heat

1. Introduction

In the floating zone (FZ) method for the growth of silicon single crystals utilized in electronic devices, it is important to understand the heat transfer mechanism in order to control the temperature field and molten zone shape, since the quality of the growing crystals depends on the shape of the interface, the thermal history in the furnace and the fluid flow in the molten zone. In recent decades, much attention has been given to heat transfer, fluid flow, interface shapes and free surface shapes in FZ silicon crystal growth [1–12]. The FZ method with a pancake induction coil or inductor (Fig. 1) has been recently introduced for the production of large silicon single crystals with diameters greater than 100 mm [8–12]. The induced eddy current, the temperature field, the radiation boundary and the feed/crystal rotation rates determine the interface shapes of the molten zone and cause the fluid flow.

* Corresponding author. Fax: +81 22 217 5243; e-mail: maruyama@ifs.tohoku.ac.jp.

0022-0248/98/$ – see front matter © 1998 Elsevier Science B.V. All rights reserved.
PII: S0022-0248(98)00752-0

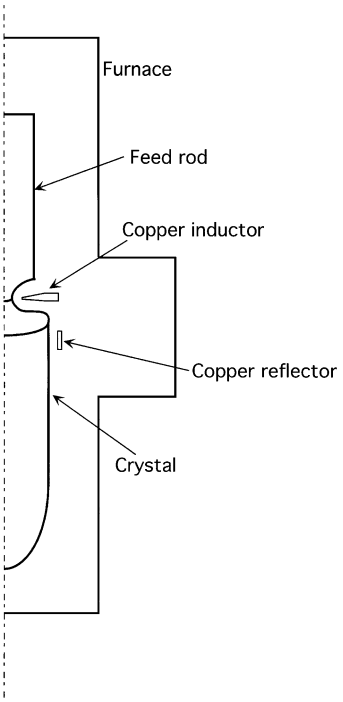

Fig. 1. Schematic sketch of the floating zone furnace with the needle-eye technique.

The presence of the relatively small inner hole of the inductor causes the existence of the melt surface including the melting front on the feed rod and the zone free surface and has a strong influence on the heat transfer and the interface shapes of the molten zone.

Radiative heat transfer is important in the calculation of temperature field and fluid flow in the FZ growth process. To obtain an accurate radiation boundary, an appropriate radiation analysis is necessary. As Guo et al. [11] point out, however, the radiative heat exchange in the previous numerical FZ works [3–10] was dealt with by neglecting the view factors associated with the surface of the sample including crystal, melt and feed rod, with the inductor and with the casing, not to mention the consideration of specular property of the Si crystal and melt surfaces against thermal radiation. Refs. [11,12] reveal that the neglecting of view factors leads to a considerable error in the prediction of radiative heat flux. Difficulties arise in calculating view factors in the FZ furnace with needle-eye technique since the structure in the zone and inductor area is too complicated for analyzing radiative transfer with specular reflection component using analytical solutions [13]. Guo et al. [11] introduced the radiation element method [14,15] based on the ray emission model [15] to solve the radiation exchange in the FZ furnace with diffuse and specular surfaces and needle-eye inductor. The radiation element method, REM2 [16] can deal with radiative heat transfer in an arbitrary system that possess both specular and/or diffuse reflection components. Using such a method, the radiation transfer in Czochralski silicon crystal growth furnaces has also been studied [15–17].

The surface radiative property (diffuse or specular) strongly influences the radiative heat transfer in the FZ furnace [11]. However, this effect has not been studied in a coupled heat transfer mode. The heat transfer and interface shape are strongly coupled with the electromagnetic (EM) field, free zone surface, heat conduction and radiation, and Joulean heat. Coriell and Cordes [1] presented the solution for the shape of the melt free surface, which involves the balance between the surface tension force and the hydrostatic pressure in the melt, and can be described by the Laplace–Young equation including EM pressure. For the FZ silicon growth with the needle-eye inductor, the free surface shape, EM field and AC electric current distribution have been investigated by Lie et al. [2]. The heat transfer and fluid flow were studied by Mühlbauer et al. [8]. The interface shape, heat transfer and thermal stress were calculated by Riemann et al. [9].

In the present work, the heat transfer, interface shape and Joulean heat in the FZ growth of large Si crystals are investigated. The objective is to study the effect of the silicon surface radiative characteristics on the heat transfer, Joulean heat and interface shape in the growth. The radiation element method is adopted to solve the radiative heat transfer with diffuse and/or specular surfaces. The distributions of applied voltage and heat flux, and the temperature fields are obtained. The interface shape is predicted and compared with the experiment. The effect of the specular reflection on the crystal and melt surfaces is scrutinized.

2. Mathematical model

2.1. EM field and free surface

In the floating zone process, the AC electric current induced by the magnetic field is confined in the vicinity of surfaces of the inductor, melt, crystal and feed rod, because of the high current frequency. In the case of silicon melt, the penetration depth is $\delta = (\pi\mu f\sigma)^{-1/2} \approx 0.3$ mm for a frequency of $f = 3$ MHz, where μ is the magnetic permeability and σ the electrical conductivity. Therefore, the peak surface AC current, $J_\theta(s)$, can be treated as

$$J_\theta(s)\cos(\omega t) = \int j_\theta \, \mathrm{d}n, \tag{1}$$

Here, j_θ is the dimensionless AC azimuthal electric current density inside the penetration depth layer. The curvilinear coordinate s and the normal direction n are demonstrated in Fig. 2.

The FZ furnace is assumed to be axisymmetric because the feed rod and crystal are rotated during the growth process. The AC magnetic field has radial and axial components B_r and B_z, and the electric field has only an azimuthal component E_θ. They can be calculated by the following expression:

$$B_r = -\frac{\partial A_\theta}{\partial z}, \quad B_z = \frac{1}{r}\frac{\partial}{\partial r}(rA_\theta), \quad E_\theta = \frac{1}{r}\frac{\partial \phi}{\partial \theta} - \frac{\partial A_\theta}{\partial t}, \tag{2}$$

where the electric potential function ϕ and the magnetic vector potential A_θ were introduced. If $r = R(s)$ and $z = Z(s)$ on the surfaces of the melt, feed rod, crystal and inductor, A_θ at any point on the surfaces due to the electric surface current is given [2]

$$A_\theta(r, z, t) = \frac{\cos(\omega t)}{\pi}\int J_\theta(s)\left(\frac{R}{mr}\right)^{1/2}[K(m) - E(m)]\,\mathrm{d}s, \tag{3}$$

in which $K(m)$ and $E(m)$ are the complete elliptic integrals of the first and second kind, respectively [2] taking $A_\theta = 0$ as the boundary condition at the surfaces of feed rod, melt and crystal since there is no applied voltage. In the inductor, an applied voltage V_0 exists, so that

$$A_\theta = \frac{V_0\cos(\omega t)}{2\pi r\omega}. \tag{4}$$

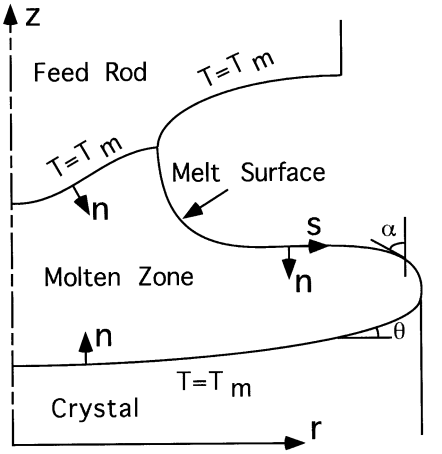

Fig. 2. Schematic diagram of the molten zone, interfaces and coordinates.

The shape of free surface on the melt zone should be determined by solving Laplace–Young equation including the EM body force [2], which is expressed as

$$\frac{\mathrm{d}R}{\mathrm{d}s} = \sin\alpha, \quad \frac{\mathrm{d}Z}{\mathrm{d}s} = \cos\alpha,$$

$$\frac{\mathrm{d}\alpha}{\mathrm{d}s} = \frac{\cos\alpha}{R} + \varepsilon Z + \frac{1}{4}\varepsilon_\mathrm{m} J_\theta^2 - P_0, \tag{5}$$

with $\varepsilon_\mathrm{m} = V_0^2/(\mu\gamma\omega^2 R_\mathrm{C}^3)$ as the EM bond number. Here, V_0 is the applied voltage, γ is the surface tension coefficient, R_C is the crystal radius, and P_0 is the difference between the interior melt pressure at $z = 0$ and the gas pressure.

2.2. Joulean heat

The EM field induces Joulean heat which is the heat source for the melting of the float zone. The body Joulean heat can be expressed as

$$Q = j_\theta^2/\sigma. \tag{6}$$

In the FZ method, the Joulean heat is generated inside the very thin penetration depth layer of the

sample, so that it can be treated as surface heat flux as boundary condition in global heat transfer. The heat flux by Joulean heat is evaluated as an averaged value of the integral of Q in the penetration depth to the normal direction over one cycle of the AC current, and it can be expressed as [18]

$$q^j = \frac{\omega}{2\pi}\int_0^{2\pi/\omega}\frac{1}{\sigma}\int j_\theta^2 \,\mathrm{d}n\,\mathrm{d}t = \frac{J_\theta^2}{2\sigma\delta}. \tag{7}$$

2.3. Radiative heat transfer

The study of Guo et al. [11] reveals that a proper analysis of radiation exchange is very important in silicon FZ process. The melt surface is generally specular against thermal radiation and is curved in shape. The surface of feed rod can be treated as diffuse. Many analytical solutions have been utilized in analyzing radiation transfer with diffuse and specular components. As Modest [13] points out, however, such methods are limited to simple geometries. For the complicated FZ furnace with diffuse and specular surfaces, it becomes a formidable task to calculate radiative exchange using conventional analytical methods. Thus, the radiative heat transfer was treated by neglecting the view factors associated with the surfaces of sample and inductor in most of the previous works. However, such a simplification leads to a significant error by one or two factors in the prediction of radiative heat flux [11]. Moreover, the specular property of the melt surface enhances the radiation transfer in the zone region. The effect of specular surfaces should be taken into account.

The radiation element method based on the ray tracing method was introduced to investigate the radiative heat transfer in FZ growth of large silicon crystals by Guo et al. [11,12]. In this method, the absorption view factor $F^{\mathrm{A}}_{i,j}$ and diffuse reflection view factor $F^{\mathrm{D}}_{i,j}$ were defined for analyzing radiation exchange by Maruyama [14]. The method has been described in the researches of Maruyama [14] and Guo et al. [15] in detail. If the furnace is comprised of N radiation elements, the diffuse radiation heat transfer rate Q_{Ji} and the net rate of heat loss Q_{Xi} of element i can be expressed as

$$Q_{Ji} = Q_{Ti} + \sum_{j=1}^{M} F^{\mathrm{D}}_{j,i}Q_{J_j},$$

$$Q_{Xi} = Q_{Ti} - \sum_{j=1}^{M} F^{\mathrm{A}}_{j,i}Q_{Jj} \tag{8}$$

in which $Q_{Ti} = A_i\varepsilon_i\sigma T_i^4$ with A as the area of surface element, ε the emissivity and σ the Stefan–Boltzmann constant. Substituting matrix $\boldsymbol{F}$ and vector $\boldsymbol{Q}$ for $F_{j,i}$ and Q_i, respectively, and eliminating Q_{Ji} from Eq. (8), the following relationship is achieved:

$$\boldsymbol{F}_X\boldsymbol{Q}_T = \boldsymbol{I}\boldsymbol{Q}_X, \tag{9}$$

where

$$\boldsymbol{F}_X = \boldsymbol{I} - \boldsymbol{F}^A(\boldsymbol{I} - \boldsymbol{F}^{\mathrm{D}})^{-1} \tag{10}$$

and $\boldsymbol{I}$ and $(\,)^{-1}$ stand for unit matrix and inverse matrix, respectively. When each element in the enclosed system has a specified temperature T_i, the unknown components of Q_{Xi} can be calculated by matrix operation of Eq. (9). The radiative heat flux q_i^{r} of element i is obtained by

$$q_i^{\mathrm{r}} = \frac{Q_{Xi}}{A_i}. \tag{11}$$

2.4. Global heat transfer

We assume that the heat transfer in the molten zone is dominated by heat conduction. The governing equation for global heat transfer in the FZ furnace can be expressed as

$$\rho_k c_{p,k}\left(\frac{\partial T_k}{\partial t} + v_k\frac{\partial T_k}{\partial z}\right) = \frac{1}{r}\frac{\partial}{\partial r}\left[r\lambda_k(T)\frac{\partial T_k}{\partial r}\right] + \frac{\partial}{\partial z}\left[\lambda_k(T)\frac{\partial T_k}{\partial z}\right], \tag{12}$$

where the subscript k indicates the crystal, melt, feed rod and other components in the furnace. ρ is the density, c_p the specific heat, λ the thermal conductivity, and v will represent the feeding velocity v_{f} in the feed rod and growth velocity v_{c} in the crystal.

The boundary conditions for the heat transfer taking into account the Joulean heat and the

radiation are given as follows:

(1) along the centerline of the system, $\partial T/\partial r = 0$, due to symmetry.

(2) On the surfaces of the feed rod, melt, and crystal

$$\lambda(T)\frac{\partial T}{\partial n} = q^{\mathrm{r}} - q^{\mathrm{j}}. \tag{13}$$

(3) At the interfaces of melting and growth, and on the open melting front in the feed rod, $T = T_{\mathrm{m}}$, with T_{m} the melting point temperature. In addition, the unknown liquid/solid interfaces are described by the heat balance conditions:

At the interface between the feed rod and melt

$$\lambda_{\mathrm{s}}\frac{\partial T}{\partial n} - \lambda_{\mathrm{l}}\frac{\partial T}{\partial n} = -v_{\mathrm{f}}\rho_{\mathrm{s}}L\cos\theta, \tag{14}$$

at the interface between the melt and crystal

$$\lambda_{\mathrm{s}}\frac{\partial T}{\partial n} - \lambda_{\mathrm{l}}\frac{\partial T}{\partial n} = v_{\mathrm{c}}\rho_{\mathrm{s}}L\cos\theta, \tag{15}$$

where the subscripts s and l stand for solid silicon and liquid silicon, respectively. L is the latent heat.

(4) On the other surfaces

$$\lambda(T)\frac{\partial T}{\partial n} = q^{\mathrm{r}}. \tag{16}$$

The temperature field and the locations of the unknown interfaces are obtained by solving Eqs. (12)–(16).

3. Numerical scheme

The boundary element method is adopted to calculate the surface electric current distribution corresponding to the EM field. The boundary surfaces of the feed rod, melt, crystal and inductor are discretized in line-boundary elements, and the values of the surface current density are obtained as a solution in each element. The solutions of zone surface shape and surface current density are coupled, which require an iteration process. The iteration involves alternating between the determination of the surface current density for a given zone surface shape, and the determination of the zone surface shape for a given current density. Detailed description about the solution can be found in Ref. [2].

The finite difference method was employed to solve the global heat transfer. The calculation grids are nonuniform, i.e., they are essentially finer near the melt/gas and the melt/solid interfaces in order to capture the abrupt temperature variations at these locations more accurately. The method and its grid arrangement have been described by Togawa et al. [18] in detail.

The radiation element method was used to calculate the radiative heat transfer. The exposed surfaces in the FZ furnace are divided into numerous radiation elements composed of axisymmetric ring elements of a part of circular disc, cylinder, cone, sphere, ellipsoid or hyperboloid. The view factors between these elements are attained by using the ray tracing method based on the ray emission model [15]. The element grid for radiative transfer is usually coarser than that for heat conduction. An interpolation method is adopted to attain radiative heat flux at each conduction node. The converged solution of the coupled heat transfer with conduction and radiation was obtained by the iteration process:

(1) calculating temperature field by conduction analysis;

(2) obtaining radiative heat flux q^{r} using known temperature distribution by solving radiation transfer;

(3) using new q^{r} as new boundary condition and returning to step (1).

For the convergence criteria, the relative variations in temperature and heat flux between two successive iterations were smaller than the preassigned accuracy levels of 10^{-4}.

In radiation analysis, once the calculation of the view factors is completed, q^{r} can be calculated only by matrix operation of Eq. (9). Thus, it is necessary to do only one time computation of the view factors and the matrix inversion of Eq. (10) in the whole iteration process. The solution of Eq. (9) is purely arithmetic and requires little CPU time. This characteristic of the present radiation transfer method is useful in saving CPU time for combined heat transfer.

4. Results and discussion

The global analysis of the combined heat transfer with conduction and radiation subjected to Joulean heat was carried out in the present investigation. Efforts are focused on identifying the influence of radiation with diffuse and/or specular surfaces on heat transfer and Joulean heating. The operation parameters were set to the process of 104.5 mm diameter silicon crystal growth. The physical and radiative properties of the Si furnace used in the present computation are given in Table 1. The thermal conductivity of the inductor is expressed by $\lambda = 410.95 - 0.03549T - 1.8363 \times 10^{-5}T^2$ W/(m K).

The surfaces of the Si melt and crystal are generally specular against thermal radiation. The upper melting front may be modeled as a specular and diffuse surface. The present method can handle this kind of combined specular and diffuse surface. To clarify the influence of the radiative characteristics of the Si melt and crystal surfaces which are either specular or diffuse, however, two cases with different surface reflection properties are employed in the present study. In case 1, all the exposed surfaces in the furnace are dealt with as diffuse, i.e., $\rho^D = 1 - \varepsilon$ and $\rho^S = 0$. In case 2, the surfaces of the melt, crystal and inductor are specular, i.e., $\rho^S = 1 - \varepsilon$ and $\rho^D = 0$, while the rest surfaces in the furnace are still treated as diffuse since the surface of feed rod is usually diffuse against thermal radiation. We identify case 1 as diffuse, and case 2 as specular in the following sections.

The effect of surface radiative properties on the EM field is discussed in Fig. 3, in which the applied voltage to the inductor is plotted against the time for diffuse and specular cases. At the smallest location of time, the calculation to determine the unknown interfaces was started, and the applied voltage was controlled to keep the position of the melt/crystal/gas triple point. It is seen that the applied voltage is rapidly increased to a very high value after the floating zone process is started, and goes down quickly to an intermediate value. Then the applied voltage decreases gradually to a steady state value. Finally, the voltage is kept at a nearly constant value as the time advances. The constant values are different for different radiative properties

Table 1
Physical properties used in computation

Melting point, T_m	1685 K
Electrical conductivity of melt, σ_M	1.0×10^6 S/m
Electrical conductivity of solid, $\sigma_{C,F}$	5.0×10^4 S/m
Electrical conductivity of inductor, σ	1.0×10^6 S/m
Thermal conductivity of melt, λ_M	67 W/(m K)
Thermal conductivity of solid, $\lambda_{C,F}$	$5.7 \times 10^5 T^{-1.41}$ W/(m K)
Specific heat for sample, $c_{p\ C,F,M}$	1000 J/(kg K)
Specific heat for inductor, c_p	400 J/(kg K)
Density of sample, $\rho_{C,F,M}$	2530 kg/m^3
Density of inductor, ρ	8920 kg/m^3
Emissivity of melt, ε_M	0.26
Emissivity of solid, $\varepsilon_{C,F}$	0.55
Emissivity of inductor, reflector and chamber	0.05
Surface tension, γ	$0.73–7 \times 10^{-5} T$ N/m
Magnetic permeability, μ	1.25×10^{-6} H/m

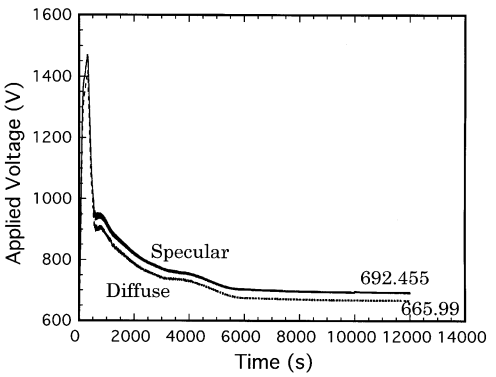

Fig. 3. The applied voltage to inductor for diffuse and specular cases.

of surface reflection. In the case of specular, the calculated applied voltage is about 5.5% larger than that for the case of diffuse in the present study.

Fig. 4a and Fig. 4b illustrate the distributions of the radiative heat flux and the net heat flux, respectively, on the Si melt surface and part of the crystal and feed rod surfaces. The net heat flux equals the radiative heat flux subtracted by the flux due to

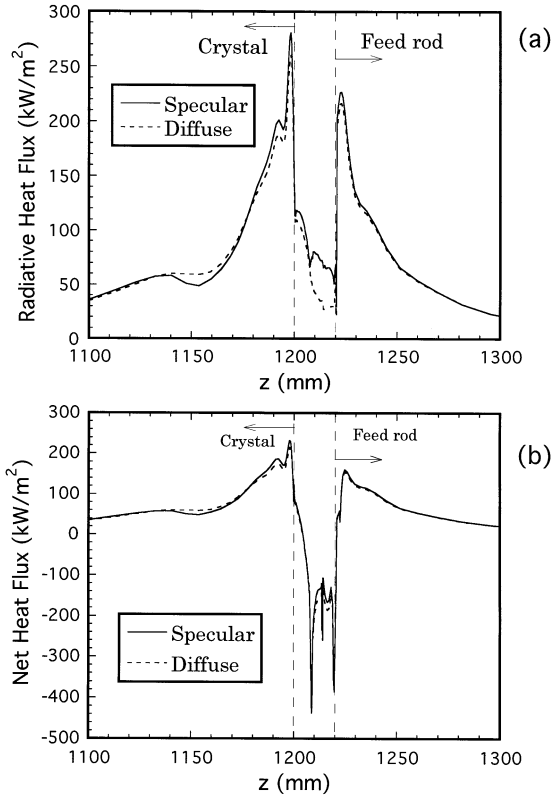

Fig. 4. Distributions of radiative heat flux (a) and net heat flux (b) in the sample via the axial coordinate for diffuse and specular cases.

Joulean heat. From Fig. 4a, it is found that the predicted radiative heat flux for the case of diffuse surfaces is much lower than that for the case of specular ones on the melt surface including melting front. This is because a diffuse system in the zone area cannot reflect radiation energy out of the zone as much as a specular system. This finding is in accordance with the research of Guo et al. [11], in which the mechanism has been studied in detail. The specular case predicts a lower radiative heat flux in one part of the crystal surface as shown in Fig. 4a. A strong specular reflecting reflector is fixed opposing to that part, which reflects radiation from the zone area back to the crystal in order to reduce the radiation heat loss. From Fig. 4b, it is seen that the net heat flux is negative in most parts of the melt in order to melt the silicon. Thus, a larger amount of Joulean heat is needed to overcome the larger radiative heat loss induced by the specular zone surface. This is why the applied voltage is larger when the specular reflection is considered as shown in Fig. 3. In the regions of crystal and feed rod, the net heat flux is positive and keeps a similar profile as in Fig. 4a. This implies that the Joulean heat is weak in these regions.

The influence of the diffuse and specular surfaces on the heat transfer and Joulean heat in the zone melt region was further examined in Fig. 5, in which the heat flux distributions were drawn via the radial coordinate. The smallest location at the r-coordinate corresponds to the feed rod/melt/gas triple point. In Fig. 5a, the calculated radiative heat flux for the case of specular is larger than that for the diffuse case in all melt locations. In particular, the prediction for specular is two to three times higher than that for diffuse in the vicinity of smaller radii, which is located at the neck area of the zone. The structure in that area is composed of the steep curvature of the melt surface and the needle-eye inductor, and makes the diffuse surface very difficult to reflect radiation out the system. The difference in the net heat flux between diffuse and specular is not very large in Fig. 5b since we try to keep the free surface, growth rate and diameter of crystal unchanged for the two different surface properties. The heat flux (absolute value) for the specular is slightly larger than that for the diffuse in most part of the molten zone.

The distributions of surface temperature are displayed in Fig. 6 for the diffuse and specular cases. From Fig. 6, it is seen that the surface temperature in specular case is larger than that in the diffuse case. The difference of temperature on the crystal surface can be as high as about 20 K. However, the difference of surface temperature between the two reflection types is not so obvious on the melt and feed rod surfaces. In the heat transfer of crystal growth process, the temperature field in the melt is of major concern. The surface temperature profiles on the melt are further demonstrated in Fig. 6b, in which the difference between the specular and diffuse is easily discovered. The largest temperature difference between the two cases is about 3 K on the melt surface. It should be noted that specular surface increases the Joulean heat and the net heat flux (absolute value) as shown in Fig. 5b, which is

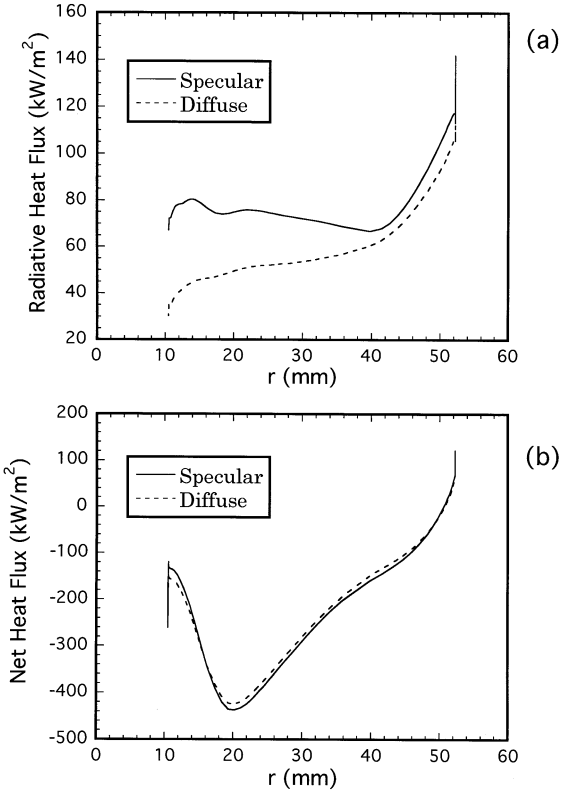

Fig. 5. Influence of surface radiative property on radiative heat flux (a) and net heat flux (b) on the melt surface via the radial coordinate.

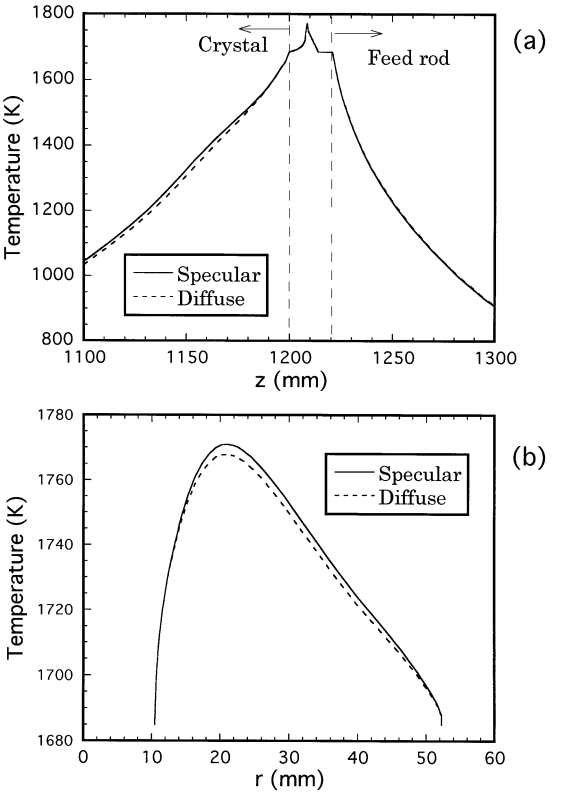

Fig. 6. Distributions of surface temperature on the sample via the axial coordinate (a) and on the melt surface via the radial coordinate (b).

the reason why the temperature is higher in the case of specular surfaces in the present study.

The interface shape between the crystal and melt is shown in Fig. 7, in which the predictions for diffuse and specular cases are compared with the experiment [19] conducted by Komatsu Electronic Metals Co., Ltd. under the same operation condition of computation. The calculated shapes of the interface are in generally good agreement with the experimental observation. The absolute values of computed depths of the zone for the specular case are larger than those of the experiment in most part of the interface. This is caused by the neglect of melt convection in the present calculation. As Mühlbauer et al. [8] pointed out, the inclusion of melt convection shortens the zone depth. It is therefore expected that the calculated shape will fit the experiment very well when both the convection and

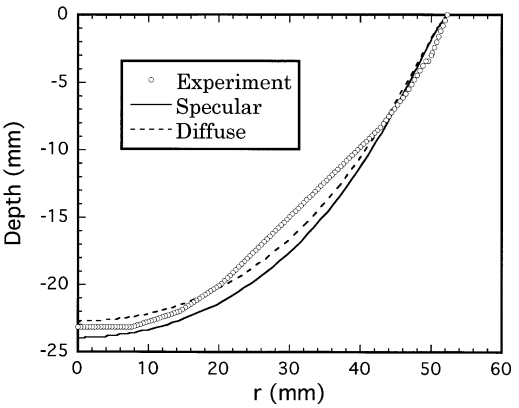

Fig. 7. Comparison of interface shapes between the experiment and the calculations in diffuse and specular cases.

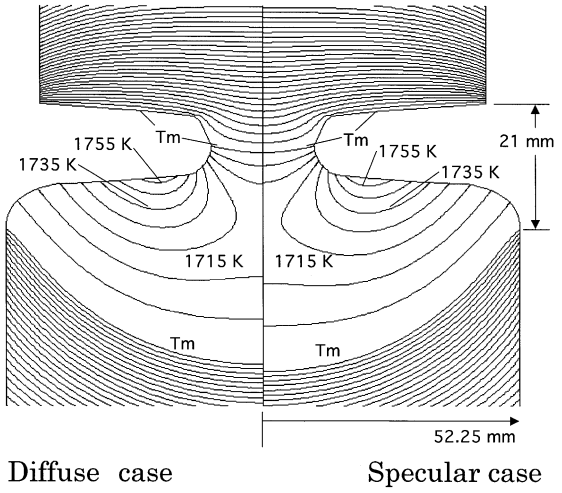

Fig. 8. Comparison of temperature fields in the sample between the diffuse and specular cases with the isotherm spacing of 10 K.

specular reflection are taken into account. Our future work will address this problem soon. As for the result in the diffuse case, the depth is shorter than that of the experiment in the central part of the interface (the area near by $r = 0$). The results for the combination of convection and diffuse are expected to deviate further the experiments. Thus, the specular character of the surface should be incorporated in Si FZ furnace.

Fig. 8 shows the temperature fields in the sample including the melt zone and parts of crystal and feed rod for the preassigned two cases of diffuse and specular. It should be borne in mind that, even in the specular case, the feed rod is still diffuse. Comparing the results between the two cases, it is found that the temperature fields in the feed rod region are rarely influenced by radiative characteristics (diffuse or specular) on the melt and crystal surfaces. However, the influence of specular reflection is obvious in the molten zone and crystal regions. When the surface specular property is incorporated, the depth of the zone is deeper and the molten zone is enlarged. Consequently, the temperature in the crystal is higher for the specular case than for the diffuse case.

5. Conclusions

Numerical analyses were carried out to delineate the combined heat transfer of radiation and conduction subjected to Joulean heat in the floating zone silicon crystal growth with needle-eye inductor, where the radiative heat transfer on surfaces with diffuse and/or specular reflection components was taken into account. The main emphasis was put on the influence of specular reflection of the surfaces of Si crystal and melt, which was often ignored by the previous researches due to the difficulty of the analysis of radiation transfer. As a result, it is found that specular reflection affects not only the radiative heat transfer, but also the combined heat transfer, Joulean heat and interface shape in the crystal growth processes.

The specular surface of the Si melt and crystal enhances the radiative heat transfer. The consideration of specular reflection increases the prediction of radiative heat flux by two to three factors on part of the melt surface compared to the case of diffuse reflection. Consequently, the Joulean heat is also influenced by the radiative characteristics of the surfaces. The specular surface requires larger Joulean heat in order to overcome the radiation heat loss. As a result, the applied voltage is augmented in the crystal growth processing when the specular reflection is accounted for.

The heat transfer is also enhanced by the use of specular property, in which the surface net heat flux is usually enlarged, the molten zone area is deepened, and the surface temperature of the melt is increased compared with the case of diffuse surfaces, and the temperature fields in the molten zone and crystal are changed. As a result, the interface shape is strongly affected by the surface reflection properties. The predicted interface shapes are in good agreement with the experimental measurement. On taking the effect of melt convection into account, the interface shape in the specular case is expected to fit the experiment much better than that in the diffuse case. A further work addressing this issue is required.

References

[1] S.R. Coriell, M.R. Cordes, J. Crystal Growth 42 (1977) 466.
[2] K.H. Lie, J.S. Walker, D.N. Riahi, J. Crystal Growth 100 (1990) 450.
[3] J.L. Duranceau, R.A. Brown, J. Crystal Growth 75 (1986) 367.

[4] C.W. Lan, S. Kou, J. Crystal Growth 108 (1991) 351.
[5] C.W. Lan, S. Kou, J. Crystal Growth 114 (1991) 517.
[6] C.W. Lan, S. Kou, J. Crystal Growth 119 (1992) 281.
[7] C.W. Lan, M.C. Liang, J. Crystal Growth 180 (1997) 381.
[8] A. Mühlbauer, A. Muiznieks, J. Virbulis, A. Lüdge, H. Riemann, J. Crystal Growth 151 (1995) 66.
[9] H. Riemann, A. Lüdge, K. Böttcher, H.-J. Rost, B. Hallmann, W. Schroder, W. Hensel, B. Schleusener, J. Electrochem. Soc. 142 (1995) 1007.
[10] A. Mühlbauer, A. Muiznieks, J. Virbulis, J. Crystal Growth 180 (1997) 372.
[11] Z. Guo, S. Maruyama, S. Togawa, JSME Int. J. 41 B (4) (1998), in press.
[12] Z. Guo, S. Maruyama, S. Togawa, 75th JSME Spring Annual Meeting V, 1998, p. 98.
[13] M.F. Modest, Radiative Heat Transfer, McGraw-Hill, New York, 1992.
[14] S. Maruyama, Numerical Heat Transfer 24 (Part A) (1993) 181.
[15] Z. Guo, S. Maruyama, T. Tsukada, Numerical Heat Transfer 32 (Part A) (1997) 595.
[16] S. Maruyama, T. Aihara, Int. J. Heat Mass Transfer 37 (1994) 1723.
[17] Z. Guo, S.-H. Hahn, S. Maruyama, T. Tsukada, 75th JSME Spring Annual Meeting III, 1998, p. 389.
[18] S. Togawa, Y. Nishi, M. Kobayashi, in: C.L. Clays, P. Rai-Choudhury, M. Watanabe, P. Stallhofer, H. J. Dowson (Eds.), High Purity Silicon V, Electrochemical Society, Pennington, NJ, 1998, to be published.
[19] S. Togawa, private communications, 1998.